 doi:10.20944/preprints202103.0044.v1

*Article*

# Presentation of the transmission functions to the mechanism of a 2T6R robot in direct kinematics, deduced by two original methods

**Liviu Marian Ungureanu [1], and Florian Ion Tiberiu Petrescu [1,*]**

[1] Bucharest Polytechnic University, "Theory of Mechanisms and Robots" Department, Bucharest, Romania, CE; ungureanu.liviu.marian@gmail.com
* Correspondence: tiberiuflorianion@gmail.com;

**Abstract:** The paper deals with the problems of direct kinematics related to a 2T6R robot, the direct kinematics of the plane mechanism of the robot. The direct kinematics of this proposed new robot help to study the movement, including the dynamic one, to determine the forces in the mechanism and to model the possible trajectories of the final effector point, thus determining the robot's working space and some of its multiple possible uses. Two totally different methods were used to verify the calculation relations, the results obtained by both methods being practically identical. The first method used is an original trigonometric method, and the second is an original geometrically analytical method.

**Keywords:** Mechanical transmissions; 2T6R robot; kinematic; direct kinematics.

## 1. Introduction

Mechanical transmissions have appeared for at least 2000 years and have had various uses, but their modern development has been strictly related to vehicles, engines, and their transmissions, and later to the development of industrial robots that began and was done on based on the requirements of the automotive industry.

The first internal combustion engine was designed in 1680 by the Dutch physicist Christian Huygens. Later, in 1807, the Swiss Francois Isaac de Rivaz designed an internal combustion engine that uses a liquid mixture of hydrogen and oxygen as fuel. At that time, the use of hydrogen as a fuel, which burns about 8-10 times faster than oil and gas fuels, was doomed to failure, because even today the direct combustion of explosive hydrogen in the engine is difficult, the tests being done most often with specialized materials unknown in the past, and for the time being there is only hydrogen burning in specialized burners with many type honeycomb cells to prevent the explosion of hydrogen. In 1824, Samuel Brown, a British engineer, adapted a steam engine to run on gasoline. It was not until 1858 that the Belgian engineer Jean Joseph Etienne Lenoir invented and patented two years later, the first two-stroke spark-ignition internal combustion engine with liquid gas (coal extract). After 3 years, the Belgian Lenoir adapted a carburetor to its engine, making it run on gasoline. In 1862, the French engineer Alphonse Beau de Rochas succeeded in designing a 4-stroke engine (patented, but not built).

The credit went to the two German engineers Eugen Langen and Nikolaus August Otto for building the theoretical model of the Rochas, the first four-stroke internal combustion engine in 1866, with electric ignition, charging and distribution in an advanced form patented ten years later by Nikolaus August Otto. In the same year (1876), the British Sir Dougald Clerk redesigned and built Lenoir's two-stroke engine, bringing it to its known form today. In 1885, Gottlieb Daimler also produced a four-stroke internal combustion engine with a single vertical cylinder with an improved carburetor.

 doi:10.20944/preprints202103.0044.v1

A year later, his compatriot Karl Benz made improvements to the four-stroke petrol engine. Daimler and Benz were working on new engines for their famous new cars. In 1889, Daimler improved the four-stroke internal combustion engine by building a "two-cylinder V" and bringing it to its classic form "with mushroom-shaped valves." It was not until 1890 that the first 4-stroke internal combustion engine was built by Wilhelm Maybach. Two years later, in 1892, the German engineer Rudolf Christian Karl Diesel invented the compression-ignition (diesel) engine.

The first valve mechanisms appeared in 1844, being used in steam locomotives, designed and built by the Belgian mechanical engineer Egide Walschaerts. The first hard memory mechanisms were designed and built in England and the Netherlands during the weaving wars. In 1719, in England, John Kay bought a five-story building, wherewith a staff of over 300 women and children, it produced the world's first weaving factory. It was not until 1750 that the textile industry was to be revolutionized by the widespread application of this invention. Initially, the weavers opposed it, destroying the flying sails and driving away from the inventor. By 1760, wars and the first automatic weaving factories appeared in the modern sense of the word. For over a century, the Italian Giovanni Branca had proposed the use of steam to drive turbines, but subsequent experiments were unsatisfactory. By the end of the 17th century, Thomas Savery had already built the "miner's friend," a steam engine that operated a pump to draw water from galleries. Thomas Newcomen made the commercial version of the steam pump, and engineer James Watt developed and adapted a cruise control that improved the engine network. Together with the manufacturer Mathiew Boulton, he built the first steam engines. In 1785 the first ship motorized with steam engines came into operation, quickly followed by several dozen.

The first distribution mechanisms appear in four-stroke car engines. In the last 25 years, a number of variants have been used to increase the number of valves per cylinder from 2 valves per cylinder, to 12 valves/cylinder, but over time it has returned to simpler versions with 2, 3, 4, or maximum 5 valves/cylinder [1].

Peugeot Citroën Group in 2006 built a hybrid engine with 4 valves with 4 cylinders, the first cam opens the normal valve and the second with phase change. Almost all current models have been stabilized at four valves per cylinder to achieve a variable distribution. In 1971, K. Hain proposed a method of optimizing the cam mechanism to obtain an optimal (maximum) transmission angle and a minimum output acceleration [2]. In 1979, F. Giordano investigated the influence of measurement errors in the kinematic analysis of the camel [3].

In 1985, P. Antonescu presented an analytical method for the synthesis of the cam mechanism and the flat barbed wire [4] and the tilt mechanism [5]. In 1988, J. Angeles and C. Lopez-Cajun presented the optimal synthesis of the cam mechanism and the oscillating plate [6]. In 2001, Dinu Taraza analyzes the influence of the cam profile, the variation of the angular velocity of the timing shaft, and the parameters of power, load, consumption, and emissions of the internal combustion engine [7].

The paper [8] presented a basic model, with one degree, with two springs, with double internal damping to simulate the movement of the cam and the drilling mechanism. The paper [9] presents the basic dynamic model of a mechanism with a cam, stick, and valve, with two degrees of freedom, without internal damping. A dynamic model with both damping in the system, external (valve spring) and internal is the one presented in the paper [10]. A dynamic model with a degree of freedom, generalized, is presented in the paper [11], in which there is also a two-degree model with double damping. In the paper [12] is proposed a dynamic model with 4 degrees of freedom, obtained as follows: the model has two moving masses, these by vertical vibration each impose a degree of freedom on which it is believed that a mass vibrates and transversely, generating another degree of freedom and the last degree of freedom is generated by the torsional torsion of the camshaft. Also, in the paper [12] is presented a simplified dynamic model, damped damping. Also in [12], there is a dynamic model, which also takes into account the torsional vibrations of the camshaft. A dynamic model with four degrees

 doi:10.20944/preprints202103.0044.v1

of freedom is presented in the paper [13], with a single oscillating table in motion, representing one of the four degrees of freedom. The other three freedoms result from a torsional deformation of the camshaft, a vertical bend (z), the camshaft, and bending deformation of the same shaft, horizontal (y), all three deformations, in a plane perpendicular to the axis of rotation. In the paper [14] are presented two dynamic models with internal damping of the system, c, variable. The determination of the internal damping of the system, c, is based on the comparison between the coefficients of the dynamic equation, written in two different ways, Newtonian and Lagrangian.

Dynamic processes in mechanical transmissions with rigid memory were studied by Petrescu and collaborators [15-23].

The INDUSTRIAL ROBOT is an integrated mechanical electronic informational system, used in the production process in order to achieve manipulation functions analogous to those performed by human hands, giving the manipulated object any freely programmed movement, within a technological process that takes place in a specific environment.

Intelligent robots represent the highest stage of development, at which the sensors are much more numerous and more complex, there are specific blocks and subsystems for moving and orienting their sensors, for measuring their movement, for processing information.

1-Trajectory generating mechanism (MGT): the mechanism formed by those kinematic couplings that make possible the displacement of the characteristic point M on the imposed trajectory. To generate the T trajectory, 3 degrees of freedom are also necessary: rotation around the Oz axis; vertical displacement along the Oz axis, and a radial displacement along the x-axis.

2-The orientation mechanism (MO) is the mechanism formed by the kinematic couplings that ensure the spatial orientation of the object, ie the mechanism that rotates after x ', y', and z '(palm-forearm of the human hand).

3-The gripping mechanism (MP) ensures the gripping and fixing of the manipulated object. If instead of handling we need welding, painting, cutting, processing, measuring ..., then the end effector will no longer be a gripper (gripping hand) but another corresponding final effector element.

Classification in terms of trajectory generation:

Robots with continuous positioning (in which the trajectory is generated continuously), which involves special blocks for correlating movements on 2 or 3 degrees of freedom, are called motion interpolators. The drive system and the control system must be suitable for this mode of operation. There must always be a well-defined bi-univocal correspondence between the command-movement. The control system must be able to manage the movements on each degree of freedom and to correlate the movements with each other, in the sense of generating the mathematically described trajectory. Controllers, sensors, motion limiters are needed, in addition to the actuation system with actuators (electric or hydraulic motors, rarely pneumatic), for actuation, command, and permanent control of the realized movement. The controller is in fact a microchip, a microprocessor, which controls the whole process of the robot, from head to tail, through system drivers some specialized programs that control all the movements of the robot, these drivers being in constant contact with the machine, system, and computer, direct and reverse connections. The control drivers perform practically all the necessary commands, in the sense that they will move from the microchip (central unit and controller) to the robot, actuators (motors) effectively commanding the necessary imposed or self-detected movements (to the latest generation intelligent robots). The drivers also check the execution of the movement by the entire robot mechanism and if the elements of the robot mechanism are in the indicated parameters (prescribed by the controller and microprocessor). In particular, the permanent positions of the end-effector end element, with the end-effector point T, its trajectory, and the sequential positions occupied in time are checked, so that they correspond to the commands given by the microprocessor, and the controller verifies their accuracy within certain prescribed limits. Whether the final element is within the prescribed limits or not is communicated by the sensors that permanently check the system parameters. There are sensors for motion, speed, acceleration, shock, tem-

Preprints (www.preprints.org) | NOT PEER-REVIEWED | Posted: 2 March 2021 doi:10.20944/preprints202103.0044.v1

perature, pressure ... The sensors give the reverse signal showing what happens to the whole system and especially to the final element end effect at any given time, and if the parameters of a point, but especially those of the final element, of the T point tracer, or effector, do not correspond at a given moment, the necessary correction is made immediately, the movement to the next step being corrected accordingly on each axis, more or less as the case may be. The role of the limiters is not to let certain moving elements exceed certain limits. For example, they will stop the rotational movement reaching a certain angle and will control the reverse movement, ie the reverse rotation to the other end where the process will be reversed again. Both motion sensors and limiters are built according to the principles of transmitters, being generally very small [24-35].

There are also robots with sequential positioning. Mechanic geometric parameters: Guide device: the set of all kinematic torques that compete to achieve the trajectories and spatial orientation of the manipulated objects within the imposed limits (MGT + MO). Final effector: clamping mechanism (in case of handling robots) or device (in case of specific operations). Load capacity: the maximum size of the mass that can be handled, in conditions of total safety, for the most unfavorable position of the robot and for the highest value of the acceleration that can develop it, in ascending vertical movement. Unfavorable position: that position of the gripping mechanism, in which the manipulated object is maintained and moved only under the effect of the frictional forces, generated by the tightening action between the object and the 'fingers' of the mechanism. Normalized load-bearing capacities: 0.250; 1; 2.5; 6.4; 10; 25; 64; 100 ... etc [36-41].

## 2. Materials and Methods

In the following, we will present a modern robot model, type 2T6R, which has multiple possibilities of movement. The bi mobile mechanism of FIG. 1 can be used in various handling applications or in technological processes. There are six movable kinematic elements and eight kinematic couplings, of which two active translation kinematic couplings A and D. The mechanism can realize with the T end of the effector 3 any curve in a certain plane domain. It is obtained from the bi mobile and bi contour kinematic chain from Fig. 2a from which derives the direct structural model (Fig. 2b) for which the base, the effector, as well as the active kinematic torques are nominated. The kinematic diagram of the 2T6R planar robot shown with two cylindrical drive motors is shown in Figure 1.

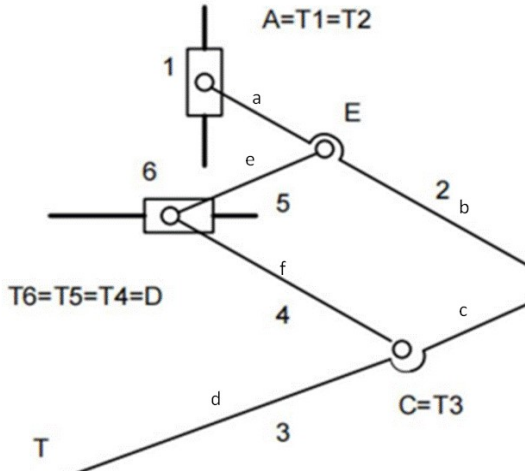


**Figure 1.** The kinematic scheme of the 2T6R plan robot presented with two cylindrical drive motors

Preprints (www.preprints.org) | NOT PEER-REVIEWED | Posted: 2 March 2021 doi:10.20944/preprints202103.0044.v1

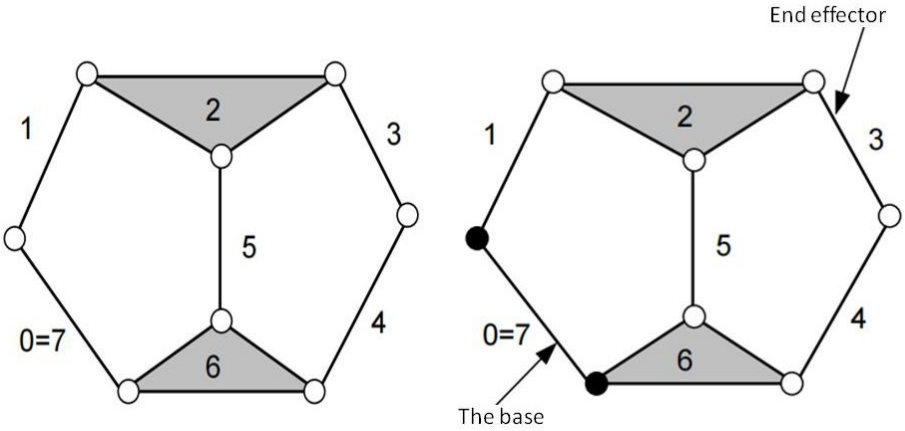


**Figure 2.** Structural scheme of the 2T6R mechanism

The connection of the modular groups (Fig. 3) corresponding to the direct structural model (Fig. 2b) comprises two initial active modular groups respectively GMAI (A, 1) and GMAI (D, 6), and two passive modular groups of dyad type, i.e. GMP1 ( 2.5) and GMP1 (3.4).

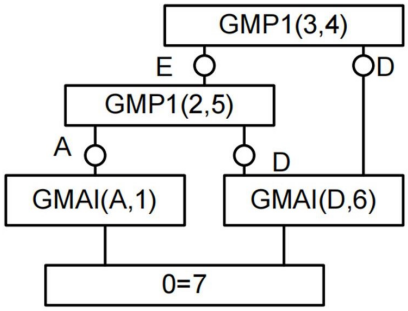


**Figure 3.** The connection of the modular groups corresponding to the direct structural model (Fig. 2b), comprises two initial active modular groups respectively GMAI (A, 1) and GMAI (D, 6), and two passive modular groups of dyad type, i.e. GMP1 ( 2.5) and GMP1 (3.4).

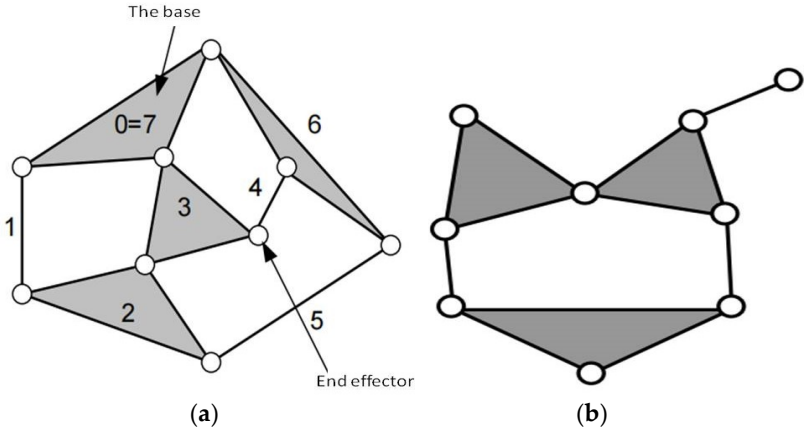


**Figure 4.** The inverse structural model (Fig. 4a) of the mechanism allows the determination of the parameters of the active torques A and D depending on the characteristics of the T point.

In the inverse structural model (Fig. 4b) the passive modular group GMP8.

Preprints (www.preprints.org) | NOT PEER-REVIEWED | Posted: 2 March 2021 doi:10.20944/preprints202103.0044.v1

The structural model directly is used to establish the algorithm for calculating the components of the reaction torque in the kinematic torques based on the kinetic-static calculation modules.

The inverse structural model (Fig. 4a) of the mechanism allows the determination of the parameters of the active torques A and D depending on the characteristics of the T point required by the technological process in which the system is used, representing the theme presented in this paper. In the inverse structural model the passive modular group GMP8 from Fig. 4b. In the connection of the groups (Fig. 5) this structure is noticeable.

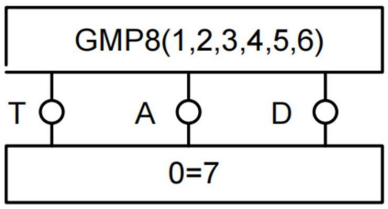


**Figure 5.** The connection of the groups GMP8(1, 2, 3, 4, 5, 6)

As we proposed in the current paper, one will initially present the direct kinematics of the 2T6R robot mechanism, verified by two completely different calculation methods: one trigonometric and a second analytical-geometric.

### *A. Kinematics by a trigonometric method*

The kinematic study begins with the determination of the positions, and then to determines the speeds and accelerations. In direct kinematics (Fig. 1) we know a, b, c, d, e, f, xA, yA, xD, yD, and must determines FI2, FI3, FI4, FI5, $x_T$, and $y_T$ are required.

#### *Dyad 2-5*

The angles FI2 and FI5 are determined first by the study of dyad 2-5 (Fig. 6), the first structural (modular) group studied.

All calculations are performed within the triangle ADE, where all the sides AE = a, DE = e, AD = $l_{AD}$ are known (the side of variable length that we determine by analytical geometric calculations). The auxiliary angle $FI_{AD}$ is also determined, two internal angles of the triangle, A and $D_1$, after which the angles $FI_2$ and $FI_5$ can be calculated directly (relations system 1).

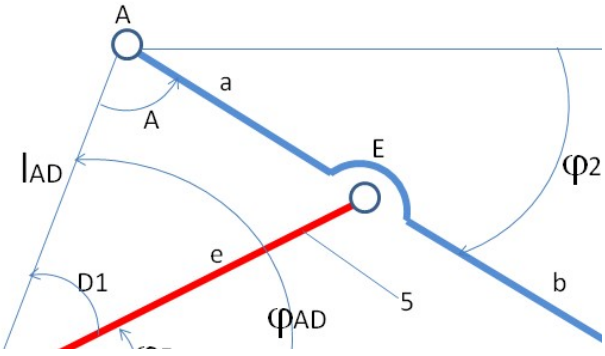


**Figure 6.** Kinematics by a trigonometric method to the dyad 2-5

Preprints (www.preprints.org) | NOT PEER-REVIEWED | Posted: 2 March 2021 doi:10.20944/preprints202103.0044.v1

$$\begin{cases} l_{AD} = \sqrt{(x_A - x_D)^2 + (y_A - y_D)^2} \\ \cos\varphi_{AD} = \dfrac{x_A - x_D}{l_{AD}}; \sin\varphi_{AD} = \dfrac{y_A - y_D}{l_{AD}} \Rightarrow \varphi_{AD} = sign(\sin\varphi_{AD}) \cdot \arccos(\cos\varphi_{AD}) \\ \cos D_1 = \dfrac{e^2 + l_{AD}^2 - a^2}{2e \cdot l_{AD}} \Rightarrow D_1 = \arccos(D_1) \Rightarrow \varphi_5 = \varphi_{AD} - D_1 \\ \cos A = \dfrac{a^2 + l_{AD}^2 - e^2}{2a \cdot l_{AD}} \Rightarrow A = \arccos(A) \Rightarrow \varphi_2 = \varphi_{AD} + A - \pi \\ x_B = x_A + (a+b) \cdot \cos\varphi_2 \\ y_B = y_A + (a+b) \cdot \sin\varphi_2 \end{cases} \quad (1)$$

In order to obtain the speeds, the positional system (1) is derived, and the relational system of speeds (2) results.

$$\begin{cases} \dot{l}_{AD} = \dfrac{(x_A - x_D) \cdot (\dot{x}_A - \dot{x}_D) + (y_A - y_D) \cdot (\dot{y}_A - \dot{y}_D)}{l_{AD}} \\ \dot{\varphi}_{AD} = \dfrac{(\dot{y}_A - \dot{y}_D) \cdot \cos\varphi_{AD} + (\dot{x}_D - \dot{x}_A) \cdot \sin\varphi_{AD}}{l_{AD}} \\ \dot{D}_1 = \dfrac{e \cdot \dot{l}_{AD} \cdot \cos D_1 - l_{AD} \cdot \dot{l}_{AD}}{e \cdot l_{AD} \cdot \sin D_1}; \quad \dot{\varphi}_5 = \dot{\varphi}_{AD} - \dot{D}_1 \\ \dot{A} = \dfrac{a \cdot \dot{l}_{AD} \cdot \cos A - l_{AD} \cdot \dot{l}_{AD}}{a \cdot l_{AD} \cdot \sin A}; \quad \dot{\varphi}_2 = \dot{\varphi}_{AD} + \dot{A} \\ \dot{x}_B = \dot{x}_A - (a+b) \cdot \sin\varphi_2 \cdot \omega_2 \\ \dot{y}_B = \dot{y}_A + (a+b) \cdot \cos\varphi_2 \cdot \omega_2 \end{cases} \quad (2)$$

The relational system (2) of velocities is derived again with time and the relational system (3) of accelerations is obtained.

$$\begin{cases} \ddot{l}_{AD} = \dfrac{(\dot{x}_A - \dot{x}_D)^2 + (\dot{y}_A - \dot{y}_D)^2 + (x_A - x_D) \cdot (\ddot{x}_A - \ddot{x}_D) + (y_A - y_D) \cdot (\ddot{y}_A - \ddot{y}_D) - \dot{l}_{AD}^2}{l_{AD}} \\ \ddot{\varphi}_{AD} = \dfrac{(\ddot{y}_A - \ddot{y}_D) \cdot \cos\varphi_{AD} + (\ddot{x}_D - \ddot{x}_A) \cdot \sin\varphi_{AD} - 2\dot{l}_{AD} \cdot \dot{\varphi}_{AD}}{l_{AD}} \\ \ddot{D}_1 = \dfrac{e \cdot \ddot{l}_{AD} \cdot \cos D_1 - 2e \cdot \dot{l}_{AD} \cdot \sin D_1 \cdot \dot{D}_1 - e \cdot l_{AD} \cdot \cos D_1 \cdot \dot{D}_1^2 - \dot{l}_{AD}^2 - l_{AD} \cdot \ddot{l}_{AD}}{e \cdot l_{AD} \cdot \sin D_1}; \\ \ddot{\varphi}_5 = \ddot{\varphi}_{AD} - \ddot{D}_1 \\ \ddot{A} = \dfrac{a \cdot \ddot{l}_{AD} \cdot \cos A - 2a \cdot \dot{l}_{AD} \cdot \sin A \cdot \dot{A} - a \cdot l_{AD} \cdot \cos A \cdot \dot{A}^2 - \dot{l}_{AD}^2 - l_{AD} \cdot \ddot{l}_{AD}}{a \cdot l_{AD} \cdot \sin A}; \\ \ddot{\varphi}_2 = \ddot{\varphi}_{AD} + \ddot{A} \\ \ddot{x}_B = \ddot{x}_A - (a+b) \cdot \cos\varphi_2 \cdot \omega_2^2 - (a+b) \cdot \sin\varphi_2 \cdot \varepsilon_2 \\ \ddot{y}_B = \ddot{y}_A - (a+b) \cdot \sin\varphi_2 \cdot \omega_2^2 + (a+b) \cdot \cos\varphi_2 \cdot \varepsilon_2 \end{cases} \quad (3)$$

***Dyad 3-4***

Preprints (www.preprints.org) | NOT PEER-REVIEWED | Posted: 2 March 2021 doi:10.20944/preprints202103.0044.v1

The angles FI3 and FI4 are determined by the study of the dyad 3-4 (Fig. 7), the second structural (modular) group studied in direct kinematics.

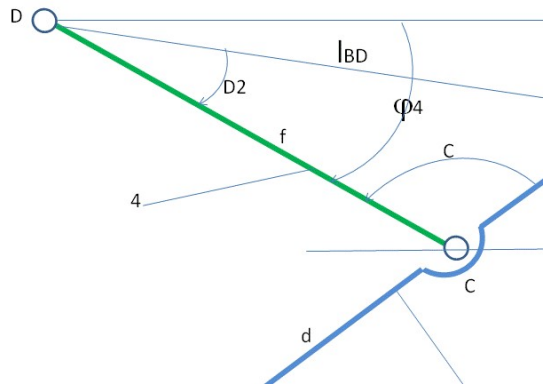


**Figure 7.** Kinematics by a trigonometric method to the dyad 3-4

Having a dyad of the same appearance as the previous, the study will be similar and will determine the positions (4), speeds (5), and accelerations (6).

$$\begin{cases} l_{BD} = \sqrt{(x_B - x_D)^2 + (y_B - y_D)^2} \\ \cos\varphi_{BD} = \dfrac{x_B - x_D}{l_{BD}}; \sin\varphi_{BD} = \dfrac{y_B - y_D}{l_{BD}} \Rightarrow \varphi_{BD} = sign(\sin\varphi_{BD}) \cdot \arccos(\cos\varphi_{BD}) \\ \cos D_2 = \dfrac{f^2 + l_{BD}^2 - c^2}{2f \cdot l_{BD}} \Rightarrow D_2 = \arccos(D_2) \Rightarrow \varphi_4 = \varphi_{BD} - D_2 \\ \cos C = \dfrac{f^2 + c^2 - l_{BD}^2}{2f \cdot c} \Rightarrow C = \arccos(C) \Rightarrow \varphi_3 = \pi + \varphi_4 - C \\ \begin{cases} x_C = x_D + f \cdot \cos\varphi_4 \\ y_C = y_D + f \cdot \sin\varphi_4 \end{cases} \begin{cases} x_T = x_C - d \cdot \cos\varphi_3 \\ y_T = y_C - d \cdot \sin\varphi_3 \end{cases} \end{cases} \quad (4)$$

$$\begin{cases} \dot{l}_{BD} = \dfrac{(x_B - x_D) \cdot (\dot{x}_B - \dot{x}_D) + (y_B - y_D) \cdot (\dot{y}_B - \dot{y}_D)}{l_{BD}} \\ \dot{\varphi}_{BD} = \dfrac{(\dot{y}_B - \dot{y}_D) \cdot \cos\varphi_{BD} + (\dot{x}_D - \dot{x}_B) \cdot \sin\varphi_{BD}}{l_{BD}} \\ \dot{D}_2 = \dfrac{f \cdot \dot{l}_{BD} \cdot \cos D_2 - l_{BD} \cdot \dot{l}_{BD}}{f \cdot l_{BD} \cdot \sin D_2} \Rightarrow \dot{\varphi}_4 = \dot{\varphi}_{BD} - \dot{D}_2 \\ \dot{C} = \dfrac{l_{BD} \cdot \dot{l}_{BD}}{f \cdot c \cdot \sin C} \Rightarrow \dot{\varphi}_3 = \dot{\varphi}_4 - \dot{C} \\ \begin{cases} \dot{x}_C = \dot{x}_D - f \cdot \sin\varphi_4 \cdot \omega_4 \\ \dot{y}_C = \dot{y}_D + f \cdot \cos\varphi_4 \cdot \omega_4 \end{cases} \begin{cases} \dot{x}_T = \dot{x}_C + d \cdot \sin\varphi_3 \cdot \omega_3 \\ \dot{y}_T = \dot{y}_C - d \cdot \cos\varphi_3 \cdot \omega_3 \end{cases} \end{cases} \quad (5)$$

Preprints (www.preprints.org) | NOT PEER-REVIEWED | Posted: 2 March 2021 doi:10.20944/preprints202103.0044.v1

$$
\begin{cases}
\ddot{l}_{BD} = \dfrac{(\dot{x}_B - \dot{x}_D)^2 + (\dot{y}_B - \dot{y}_D)^2 + (x_B - x_D)\cdot(\ddot{x}_B - \ddot{x}_D) + (y_B - y_D)\cdot(\ddot{y}_B - \ddot{y}_D) - \dot{l}_{BD}^2}{l_{BD}} \\
\ddot{\varphi}_{BD} = \dfrac{(\ddot{y}_B - \ddot{y}_D)\cdot\cos\varphi_{BD} + (\ddot{x}_D - \ddot{x}_B)\cdot\sin\varphi_{BD} - 2\dot{l}_{BD}\cdot\dot{\varphi}_{BD}}{l_{BD}} \\
\ddot{D}_2 = \dfrac{f\cdot\ddot{l}_{BD}\cdot\cos D_2 - 2f\cdot\dot{l}_{BD}\cdot\sin D_2\cdot\dot{D}_2 - f\cdot l_{AD}\cdot\cos D_2\cdot\dot{D}_2^2 - \dot{l}_{BD}^2 - l_{BD}\cdot\ddot{l}_{BD}}{f\cdot l_{BD}\cdot\sin D_2} \\
\ddot{\varphi}_4 = \ddot{\varphi}_{BD} - \ddot{D}_2 \\
\ddot{C} = \dfrac{\dot{l}_{BD}^2 + l_{BD}\cdot\ddot{l}_{BD} - f\cdot c\cdot\cos C\cdot\dot{C}^2}{f\cdot c\cdot\sin C} \\
\ddot{\varphi}_3 = \ddot{\varphi}_4 - \ddot{C} \\
\\
\ddot{x}_C = \ddot{x}_D - f\cdot\cos\varphi_4\cdot\omega_4^2 - f\cdot\sin\varphi_4\cdot\varepsilon_4 \\
\ddot{y}_C = \ddot{y}_D - f\cdot\sin\varphi_4\cdot\omega_4^2 + f\cdot\cos\varphi_4\cdot\varepsilon_4 \\
\\
\ddot{x}_T = \ddot{x}_C + d\cdot\cos\varphi_3\cdot\omega_3^2 + d\cdot\sin\varphi_3\cdot\varepsilon_3 \\
\ddot{y}_T = \ddot{y}_C + d\cdot\sin\varphi_3\cdot\omega_3^2 - d\cdot\cos\varphi_3\cdot\varepsilon_3
\end{cases}
\tag{6}
$$

### *B. Kinematics by a geometric analytical method*

The kinematic study begins with the determination of the positions, and then to determines the speeds and accelerations. In direct kinematics (Fig. 1) we know a, b, c, d, e, f, xA, yA, xD, yD, and must determines FI2, FI3, FI4, FI5, $x_T$, and $y_T$ are required.

#### *Dyad 2-5*

The angles FI2 and FI5 are determined first by the study of dyad 2-5 (Fig. 8), the first structural (modular) group studied.

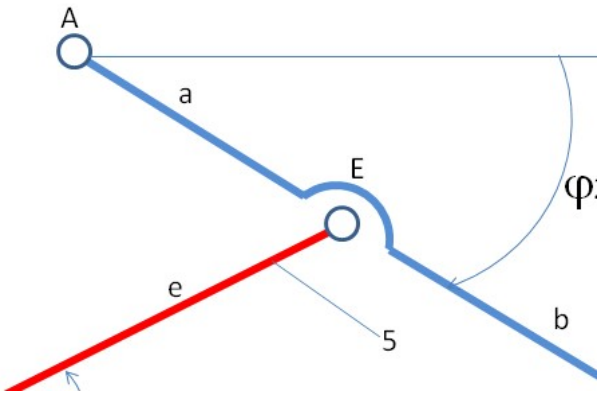


**Figure 8.** Kinematics by a geometric analytical method to the dyad 2-5

Unlike the trigonometric method where the two necessary angles are directly determined and then the inner couple of the dyad can be calculated, the geometric analyti-

Preprints (www.preprints.org) | NOT PEER-REVIEWED | Posted: 2 March 2021 doi:10.20944/preprints202103.0044.v1

cal method first determines the parameters of the inner couple (joint) of the modular group and only then can be easily determined all parameters (required angles). The analytical geometric method is much more precise regardless of the orientation of the 3R modular group, it does not depend on the positions of the elements and of the couple, or on their orientation or angles. From this point of view, the geometric analytical method is much more precise. The positions are calculated by the analytical geometric method with the help of the relations in the system (7).

$$\begin{cases} k_1 = \dfrac{x_D^2 + y_D^2 - (x_A^2 + y_A^2) + a^2 - e^2}{2 \cdot (x_D - x_A)}; \quad k_2 = \dfrac{y_D - y_A}{x_D - x_A} \\ y_E = \dfrac{k_1 \cdot k_2 - x_D \cdot k_2 + y_D \mp \sqrt{(k_1 \cdot k_2 - x_D \cdot k_2 + y_D)^2 + (1 + k_2^2) \cdot (2x_D \cdot k_1 + e^2 - x_D^2 - y_D^2 - k_1^2)}}{1 + k_2^2} \\ x_E = k_1 - k_2 \cdot y_E \\ \cos\varphi_2 = \dfrac{x_E - x_A}{a}; \sin\varphi_2 = \dfrac{y_E - y_A}{a} \Rightarrow \varphi_2 = sign(\sin\varphi_2) \cdot \arccos(\cos\varphi_2) \\ \cos\varphi_5 = \dfrac{x_E - x_D}{e}; \sin\varphi_5 = \dfrac{y_E - y_D}{e} \Rightarrow \varphi_5 = sign(\sin\varphi_5) \cdot \arccos(\cos\varphi_5) \end{cases} \tag{7}$$

$$\begin{cases} \begin{cases} (x_E - x_A)^2 + (y_E - y_A)^2 = a^2 \\ (x_E - x_D)^2 + (y_E - y_D)^2 = e^2 \end{cases} \\ \begin{cases} 2(x_E - x_A) \cdot (\dot{x}_E - \dot{x}_A) + 2(y_E - y_A) \cdot (\dot{y}_E - \dot{y}_A) = 0 \\ 2(x_E - x_D) \cdot (\dot{x}_E - \dot{x}_D) + 2(y_E - y_D) \cdot (\dot{y}_E - \dot{y}_D) = 0 \end{cases} \\ \begin{cases} (x_E - x_A) \cdot \dot{x}_E + (y_E - y_A) \cdot \dot{y}_E = (x_E - x_A) \cdot \dot{x}_A + (y_E - y_A) \cdot \dot{y}_A \\ (x_E - x_D) \cdot \dot{x}_E + (y_E - y_D) \cdot \dot{y}_E = (x_E - x_D) \cdot \dot{x}_D + (y_E - y_D) \cdot \dot{y}_D \end{cases} \\ \begin{cases} a_{11} \cdot \dot{x}_E + a_{12} \cdot \dot{y}_E = a_1 \\ a_{21} \cdot \dot{x}_E + a_{22} \cdot \dot{y}_E = a_2 \end{cases} \\ \begin{cases} a_{11} = x_E - x_A; \quad a_{12} = y_E - y_A; \quad a_1 = a_{11} \cdot \dot{x}_A + a_{12} \cdot \dot{y}_A \\ a_{21} = x_E - x_D; \quad a_{22} = y_E - y_D; \quad a_2 = a_{21} \cdot \dot{x}_D + a_{22} \cdot \dot{y}_D \end{cases} \\ \begin{cases} \Delta = a_{11} \cdot a_{22} - a_{12} \cdot a_{21} \\ \Delta_x = a_1 \cdot a_{22} - a_{12} \cdot a_2 \\ \Delta_y = a_{11} \cdot a_2 - a_1 \cdot a_{21} \end{cases} \Rightarrow \begin{cases} \dot{x}_E = \dfrac{\Delta_x}{\Delta} \\ \dot{y}_E = \dfrac{\Delta_y}{\Delta} \end{cases} \\ \omega_2 = \dfrac{(\dot{y}_E - \dot{y}_A) \cdot \cos\varphi_2 - (\dot{x}_E - \dot{x}_A) \cdot \sin\varphi_2}{a} \\ \omega_5 = \dfrac{(\dot{y}_E - \dot{y}_D) \cdot \cos\varphi_5 - (\dot{x}_E - \dot{x}_D) \cdot \sin\varphi_5}{e} \end{cases} \tag{8}$$

For such systems, there are physically two possible solutions, and if the convenient solution from angles was chosen for the trigonometric method, here things are much

Preprints (www.preprints.org) | NOT PEER-REVIEWED | Posted: 2 March 2021 doi:10.20944/preprints202103.0044.v1

simpler and more direct. We know if the constructive solution that suits us has the highest position (then we choose the + sign), or on the contrary the lowest position (in which case we choose the - sign when determining $y_E$). The velocities are determined by deriving the initial system of equations (8). The equations used in the analytical geometric method are two equations of circles with radius a and e. By deriving the position equations we obtain the velocities system which is a linear system of two equations with two unknowns, which is easily solved with Kramer, using the system determinants (8). In order to obtain the acceleration equations (9), the velocity system (8) is derived in relation to time.

$$\begin{cases} \begin{cases} a_{11}\cdot\ddot{x}_E + a_{12}\cdot\ddot{y}_E = b_1 \\ a_{21}\cdot\ddot{x}_E + a_{22}\cdot\ddot{y}_E = b_2 \end{cases} \\ \begin{cases} b_1 = a_{11}\cdot\ddot{x}_A + a_{12}\cdot\ddot{y}_A - (\dot{x}_E-\dot{x}_A)^2 - (\dot{y}_E-\dot{y}_A)^2 \\ b_2 = a_{21}\cdot\ddot{x}_D + a_{22}\cdot\ddot{y}_D - (\dot{x}_E-\dot{x}_D)^2 - (\dot{y}_E-\dot{y}_D)^2 \end{cases} \\ \begin{cases} \Delta = a_{11}\cdot a_{22} - a_{12}\cdot a_{21} \\ \Delta_{x1} = b_1\cdot a_{22} - a_{12}\cdot b_2 \\ \Delta_{y1} = a_{11}\cdot b_2 - b_1\cdot a_{21} \end{cases} \Rightarrow \begin{cases} \ddot{x}_E = \dfrac{\Delta_{x1}}{\Delta} \\ \ddot{y}_E = \dfrac{\Delta_{y1}}{\Delta} \end{cases} \\ \varepsilon_2 = \dfrac{(\ddot{y}_E-\ddot{y}_A)\cdot\cos\varphi_2 - (\ddot{x}_E-\ddot{x}_A)\cdot\sin\varphi_2}{a} \\ \varepsilon_5 = \dfrac{(\ddot{y}_E-\ddot{y}_D)\cdot\cos\varphi_5 - (\ddot{x}_E-\ddot{x}_D)\cdot\sin\varphi_5}{e} \end{cases} \quad (9)$$

***Dyad 3-4***

The angles FI3 and FI4 are determined then by the study of dyad 3-4 (Fig. 9), the second structural (modular) group studied. Repeat the calculations from the previously presented dyad, and obtain the equations of positions (10), velocities (11), and accelerations (12).

$$\begin{cases} k_{1*} = \dfrac{x_D^2 + y_D^2 - (x_B^2 + y_B^2) + c^2 - f^2}{2\cdot(x_D - x_B)}; \quad k_{2*} = \dfrac{y_D - y_B}{x_D - x_B} \\ y_C = \dfrac{k_{1*}k_{2*} - x_D k_{2*} + y_D \mp \sqrt{(k_{1*}k_{2*} - x_D k_{2*} + y_D)^2 + (1+k_{2*}^2)\cdot(2x_D k_{1*} + f^2 - x_D^2 - y_D^2 - k_{1*}^2)}}{1+k_{2*}^2} \\ x_C = k_{1*} - k_{2*}\cdot y_C \\ \cos\varphi_3 = \dfrac{x_B - x_C}{c}; \sin\varphi_3 = \dfrac{y_B - y_C}{c} \Rightarrow \varphi_3 = sign(\sin\varphi_3)\cdot\arccos(\cos\varphi_3) \\ \cos\varphi_4 = \dfrac{x_C - x_D}{f}; \sin\varphi_4 = \dfrac{y_C - y_D}{f} \Rightarrow \varphi_4 = sign(\sin\varphi_4)\cdot\arccos(\cos\varphi_4) \end{cases} \quad (10)$$

Preprints (www.preprints.org) | NOT PEER-REVIEWED | Posted: 2 March 2021 doi:10.20944/preprints202103.0044.v1

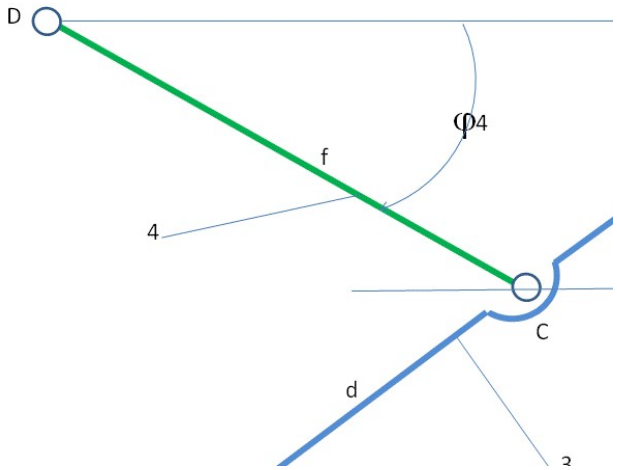


**Figure 9.** Kinematics by a geometric analytical method to the dyad 3-4

$$
\begin{cases}
\begin{cases}(x_C-x_D)^2+(y_C-y_D)^2=f^2\\(x_B-x_C)^2+(y_B-y_C)^2=c^2\end{cases}\\
\begin{cases}2(x_C-x_D)\cdot(\dot{x}_C-\dot{x}_D)+2(y_C-y_D)\cdot(\dot{y}_C-\dot{y}_D)=0\\2(x_B-x_C)\cdot(\dot{x}_B-\dot{x}_C)+2(y_B-y_C)\cdot(\dot{y}_B-\dot{y}_C)=0\end{cases}\\
\begin{cases}(x_C-x_D)\cdot\dot{x}_C+(y_C-y_D)\cdot\dot{y}_C=(x_C-x_D)\cdot\dot{x}_D+(y_C-y_D)\cdot\dot{y}_D\\(x_B-x_C)\cdot\dot{x}_C+(y_B-y_C)\cdot\dot{y}_C=(x_B-x_C)\cdot\dot{x}_B+(y_B-y_C)\cdot\dot{y}_B\end{cases}\\
\begin{cases}a_{11*}\cdot\dot{x}_C+a_{12*}\cdot\dot{y}_C=a_{1*}\\a_{21*}\cdot\dot{x}_C+a_{22*}\cdot\dot{y}_C=a_{2*}\end{cases}\\
\begin{cases}a_{11*}=x_C-x_D;\quad a_{12*}=y_C-y_D;\quad a_{1*}=a_{11*}\cdot\dot{x}_D+a_{12*}\cdot\dot{y}_D\\a_{21*}=x_C-x_B;\quad a_{22*}=y_C-y_B;\quad a_{2*}=a_{21*}\cdot\dot{x}_B+a_{22*}\cdot\dot{y}_B\end{cases}\\
\begin{cases}\Delta_*=a_{11*}\cdot a_{22*}-a_{12*}\cdot a_{21*}\\\Delta_{x*}=a_{1*}\cdot a_{22*}-a_{12*}\cdot a_{2*}\\\Delta_{y*}=a_{11*}\cdot a_{2*}-a_{1*}\cdot a_{21*}\end{cases}\Rightarrow\begin{cases}\dot{x}_C=\dfrac{\Delta_{x*}}{\Delta_*}\\\dot{y}_C=\dfrac{\Delta_{y*}}{\Delta_*}\end{cases}\\
\omega_3=\dfrac{(\dot{y}_B-\dot{y}_C)\cdot\cos\varphi_3-(\dot{x}_B-\dot{x}_C)\cdot\sin\varphi_3}{c}\\
\omega_4=\dfrac{(\dot{y}_C-\dot{y}_D)\cdot\cos\varphi_4-(\dot{x}_C-\dot{x}_D)\cdot\sin\varphi_3}{f}
\end{cases}
\tag{11}
$$

Preprints (www.preprints.org) | NOT PEER-REVIEWED | Posted: 2 March 2021 doi:10.20944/preprints202103.0044.v1

$$
\begin{cases}
\begin{cases} a_{11*}\cdot \ddot{x}_C + a_{12*}\cdot \ddot{y}_C = b_{1*} \\ a_{21*}\cdot \ddot{x}_C + a_{22*}\cdot \ddot{y}_C = b_{2*} \end{cases} \\
\begin{cases} b_{1*} = a_{11*}\cdot \ddot{x}_D + a_{12*}\cdot \ddot{y}_D - (\dot{x}_C - \dot{x}_D)^2 - (\dot{y}_C - \dot{y}_D)^2 \\ b_{2*} = a_{21*}\cdot \ddot{x}_B + a_{22*}\cdot \ddot{y}_B - (\dot{x}_C - \dot{x}_B)^2 - (\dot{y}_C - \dot{y}_B)^2 \end{cases} \\
\begin{cases} \Delta_* = a_{11*}\cdot a_{22*} - a_{12*}\cdot a_{21*} \\ \Delta_{x1*} = b_{1*}\cdot a_{22*} - a_{12*}\cdot b_{2*} \\ \Delta_{y1*} = a_{11*}\cdot b_{2*} - b_{1*}\cdot a_{21*} \end{cases} \Rightarrow \begin{cases} \ddot{x}_C = \dfrac{\Delta_{x1*}}{\Delta_*} \\ \ddot{y}_C = \dfrac{\Delta_{y1*}}{\Delta_*} \end{cases} \\
\varepsilon_3 = \dfrac{(\ddot{y}_B - \ddot{y}_C)\cdot\cos\varphi_3 - (\ddot{x}_B - \ddot{x}_C)\cdot\sin\varphi_3}{c} \\
\varepsilon_4 = \dfrac{(\ddot{y}_C - \ddot{y}_D)\cdot\cos\varphi_4 - (\ddot{x}_C - \ddot{x}_D)\cdot\sin\varphi_4}{f}
\end{cases} \tag{12}
$$

## 3. Results and discussion

The constant geometric parameters of the mechanism of Figs. 1 are listed in Table 1.

**Table 1.** Constant geometric parameters

| The constant | The value |
|---|---|
| TB = c+d | 1. |
| TC = d | 0.8 |
| AE = a | 0.3 |
| EB = b | 0.8 |
| AB = a+b | 1.1 |
| DC = f | 0.8 |
| DE = e | 0.3 |
| XA | 0. |
| YD | 0. |

Figure 10 shows the variation diagram of the four angles sought, depending on the time (input parameter), which is considered in seconds, the variation being simulated from second to second over a period of 300 seconds.

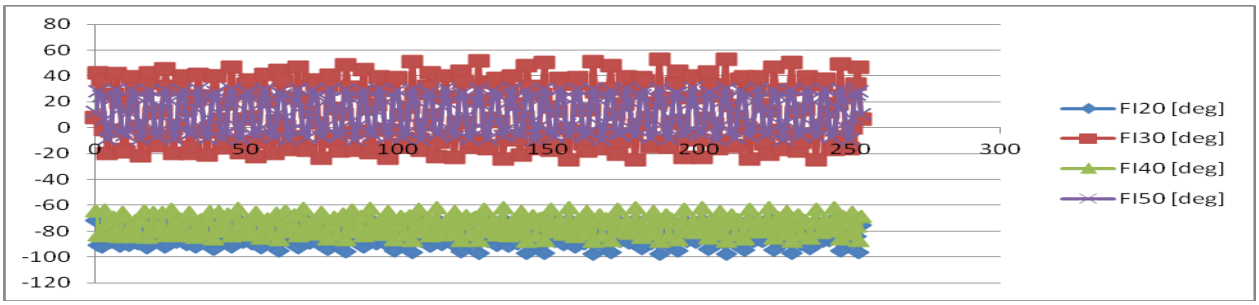


**Figure 10.** The variation of the four angles: FI2, FI3, FI4, and Fi5, in relation to the time.

Preprints (www.preprints.org) | NOT PEER-REVIEWED | Posted: 2 March 2021 doi:10.20944/preprints202103.0044.v1

In order to be able to see better the variation of the four angles, a detail made for only 15 seconds is presented in figure 11.

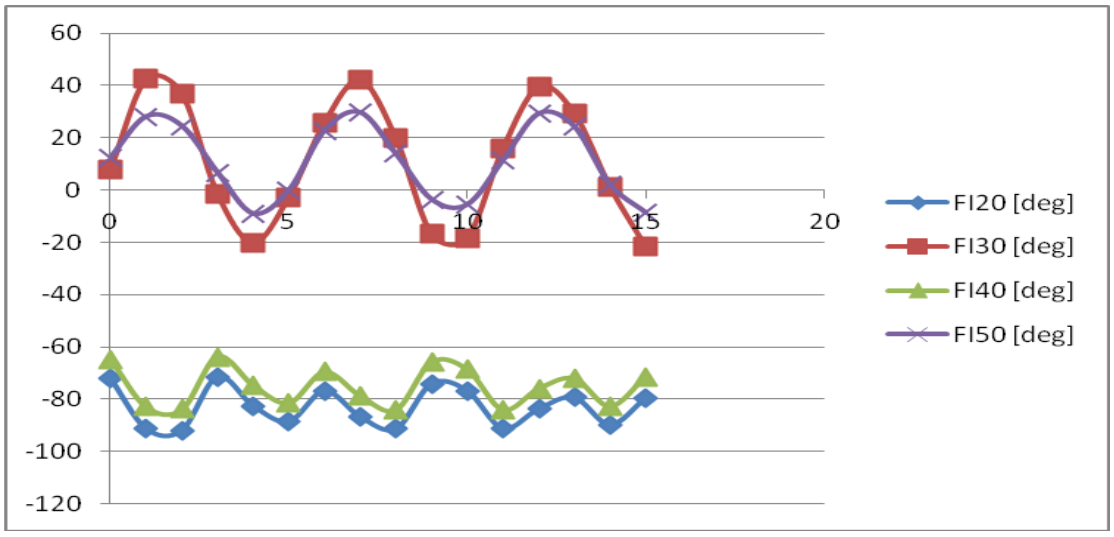


**Figure 11.** The variation of the four angles: FI2, FI3, FI4, and Fi5, in relation to the time.

The time being long enough (300 s) in relation to the working speed of the main piston 1 [1 m / s], within the complex diagram in figure 10 the vibration of the angular system of the 2T6R robot mechanism can be observed. The scalar parameters of the three couplings B, C, and E, can be followed in figure 12, in relation to the time t given in seconds.

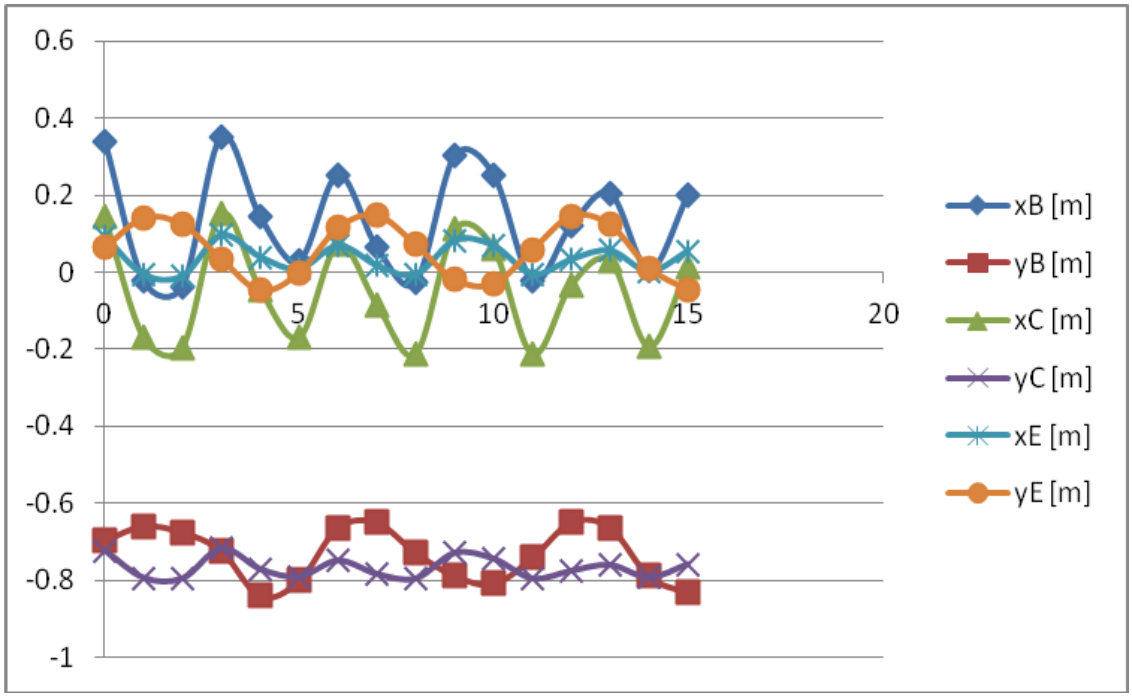


**Figure 12.** Variation of the scalar parameters of the three couplings B, C, and E.

The $x_T$, $y_T$ hodograph, represented for a longer period of time of about 300 s, generates the working space of the 2T6R robot, visible in figure 13.

Preprints (www.preprints.org) | NOT PEER-REVIEWED | Posted: 2 March 2021 doi:10.20944/preprints202103.0044.v1

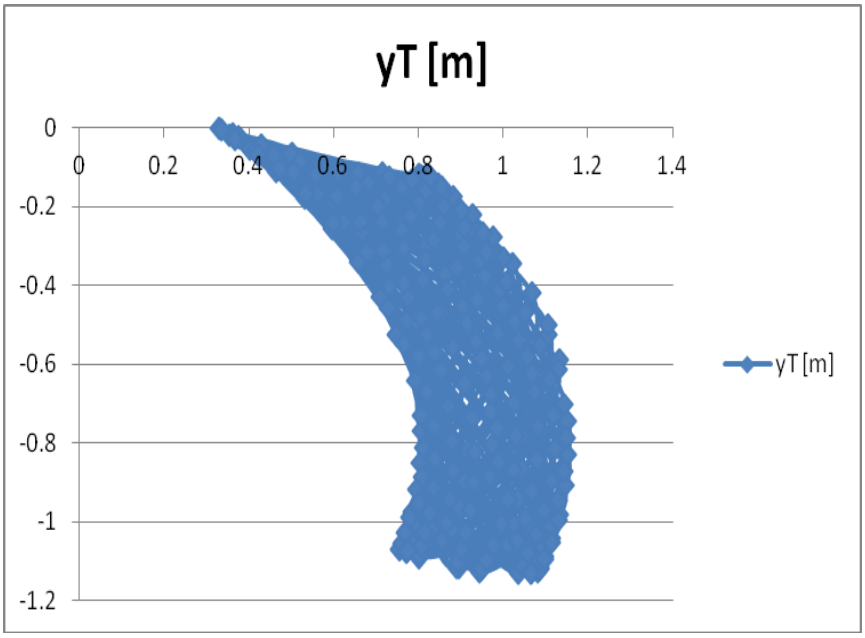


**Figure 13.** The xT, yT hodograph, represented for a longer period of time of about 300 s, generates the working space of the 2T6R robot

The angular velocities of the elements 2, 3, 4, 5, can be followed in figure 14.

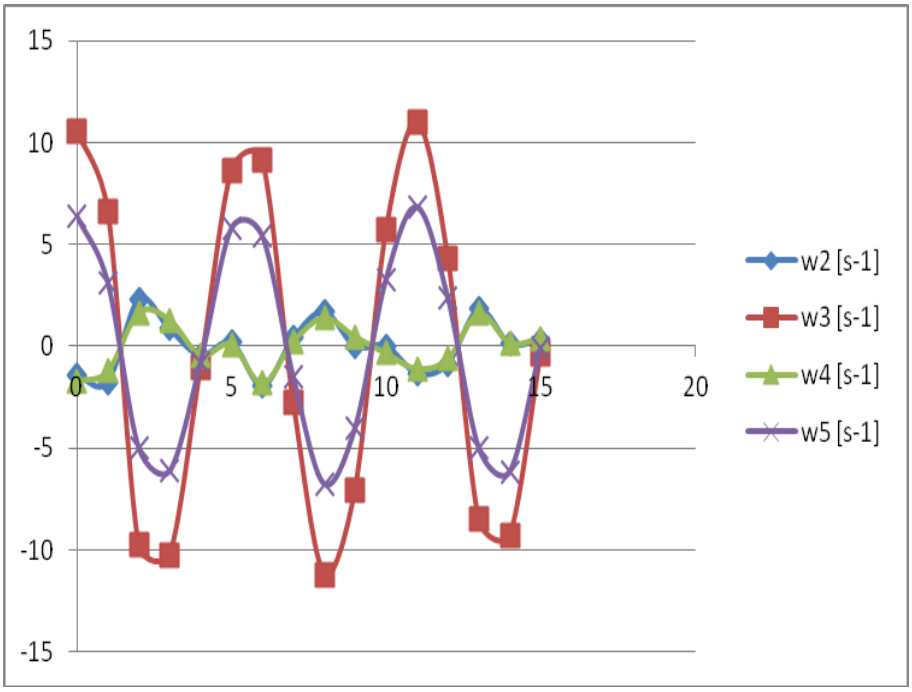


**Figure 14.** The angular velocities of the elements 2, 3, 4, and 5

Since the angular velocities of elements 2 and 4 have relatively close values, we will present in figure 15 a detail of them.

Preprints (www.preprints.org) | NOT PEER-REVIEWED | Posted: 2 March 2021 doi:10.20944/preprints202103.0044.v1

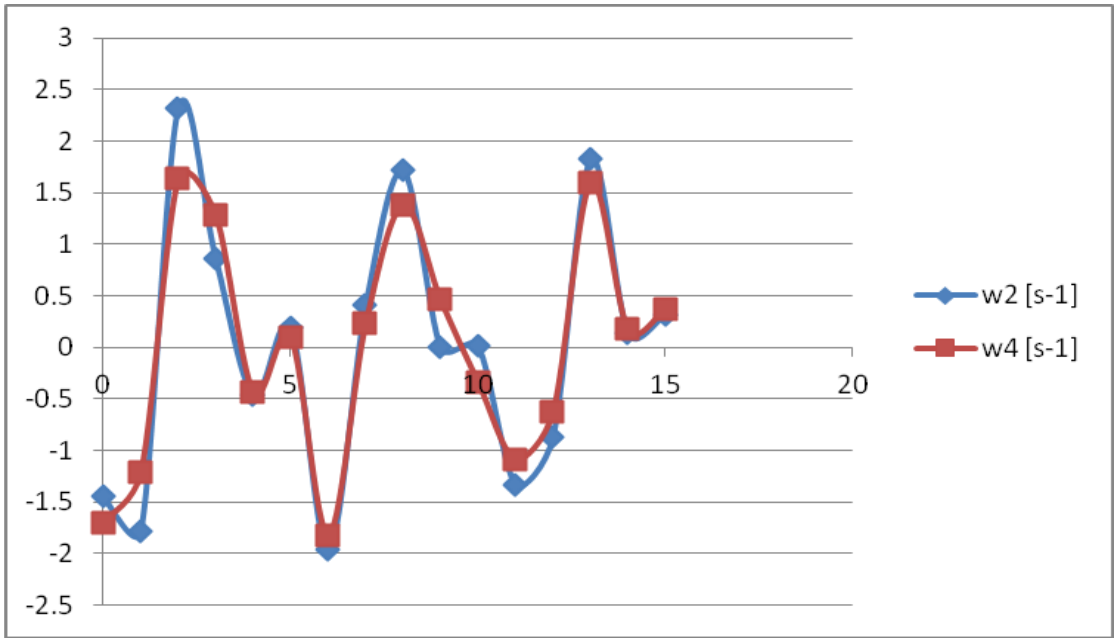


**Figure 15.** The angular velocities of the elements 2, and 4

The angular accelerations of the moving elements 2, 3, 4, and 5, will be represented in the diagram in figure 16.

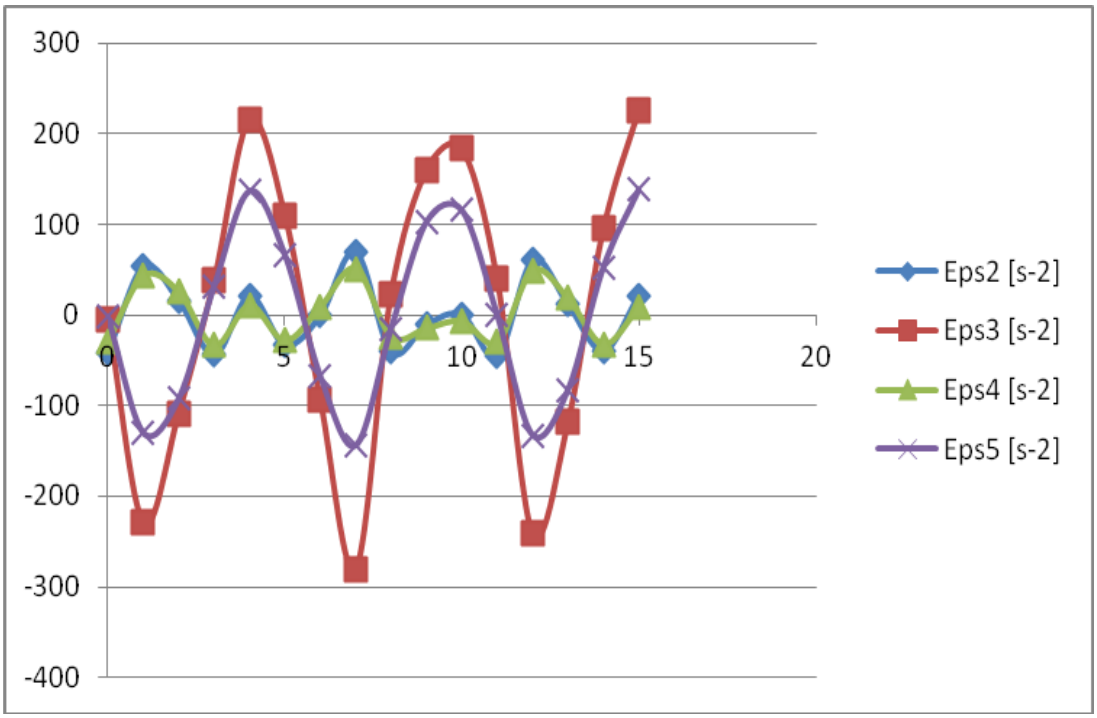


**Figure 16.** The angular accelerations of the moving elements 2, 3, 4, and 5

Since the angular accelerations of elements 2 and 4 have relatively close values, they will benefit from a detail given in the diagram in figure 17.

Preprints (www.preprints.org) | NOT PEER-REVIEWED | Posted: 2 March 2021 doi:10.20944/preprints202103.0044.v1

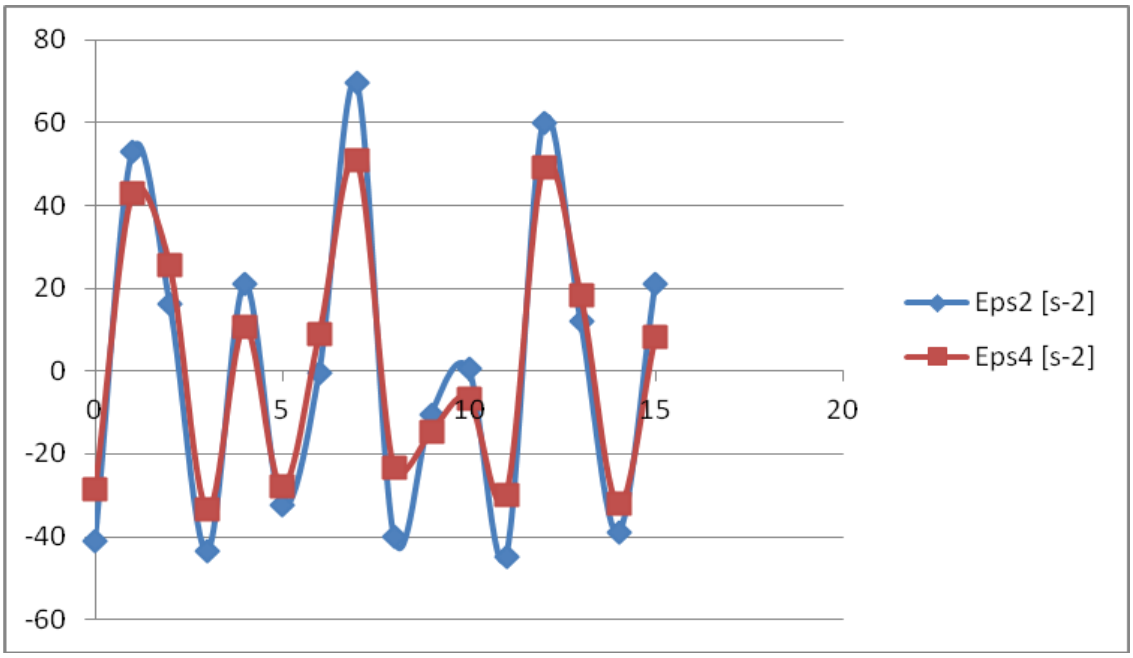


**Figure 17.** The angular accelerations of the moving elements 2 and 4

The velocities of points B, C, and E, will be represented in the diagram in figure 18.

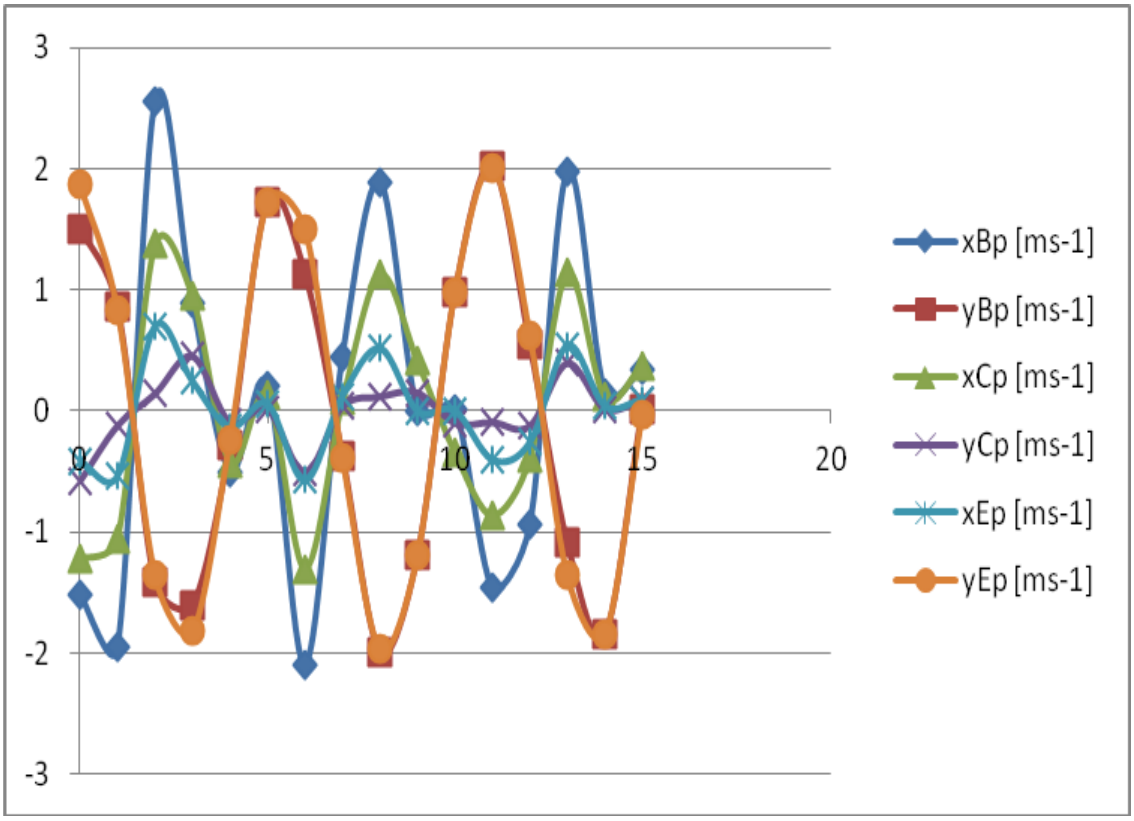


**Figure 18.** The velocities of points B, C, and E

Preprints (www.preprints.org) | NOT PEER-REVIEWED | Posted: 2 March 2021 doi:10.20944/preprints202103.0044.v1

The accelerations of points B, C, and E, will be represented in the diagram in figure 19.

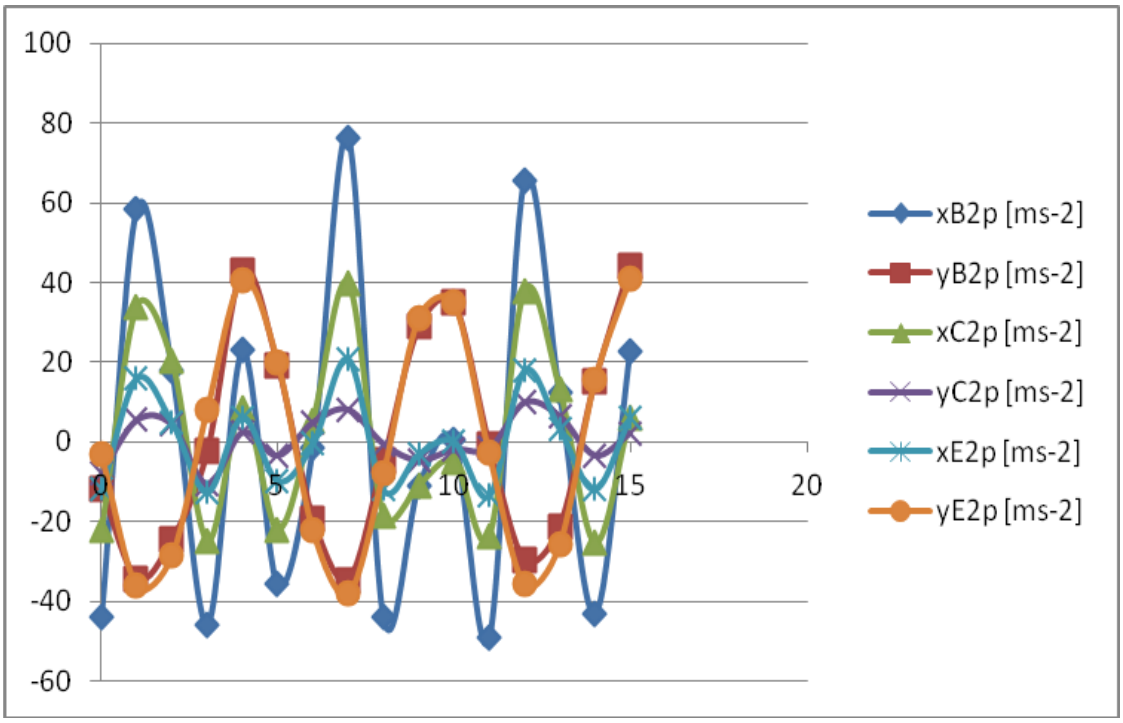


**Figure 19.** The accelerations of points B, C, and E

The velocities of the coordinates of the point T end effector will be able to be visualized within the diagram from figure 20, and the accelerations corresponding to the same endpoint will be presented in figure 21.

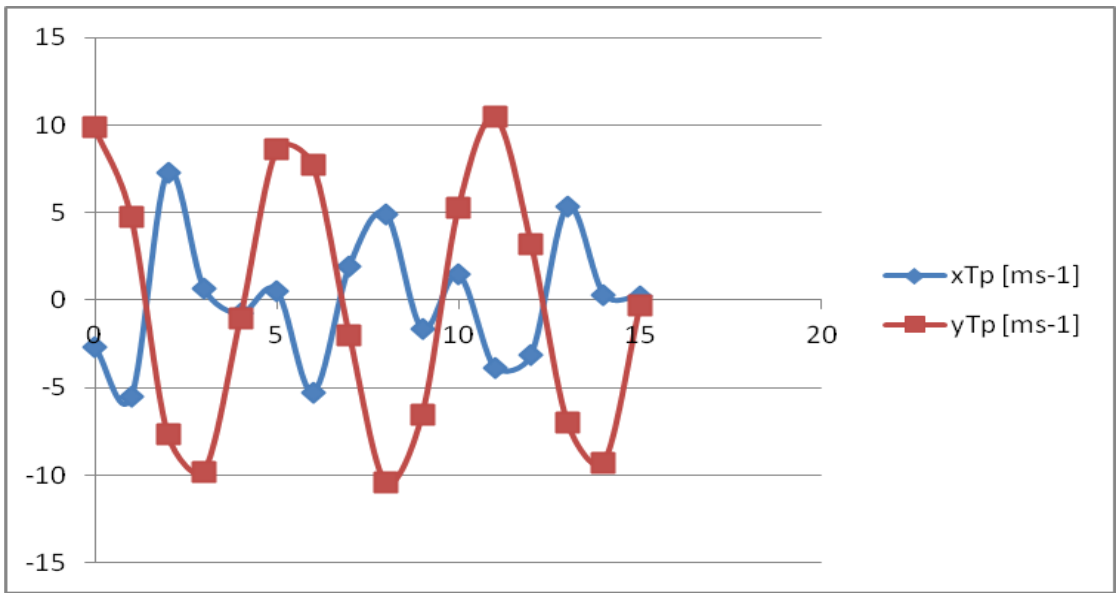


**Figure 20.** The velocities of the coordinates of the point T end effector

Preprints (www.preprints.org) | NOT PEER-REVIEWED | Posted: 2 March 2021 doi:10.20944/preprints202103.0044.v1

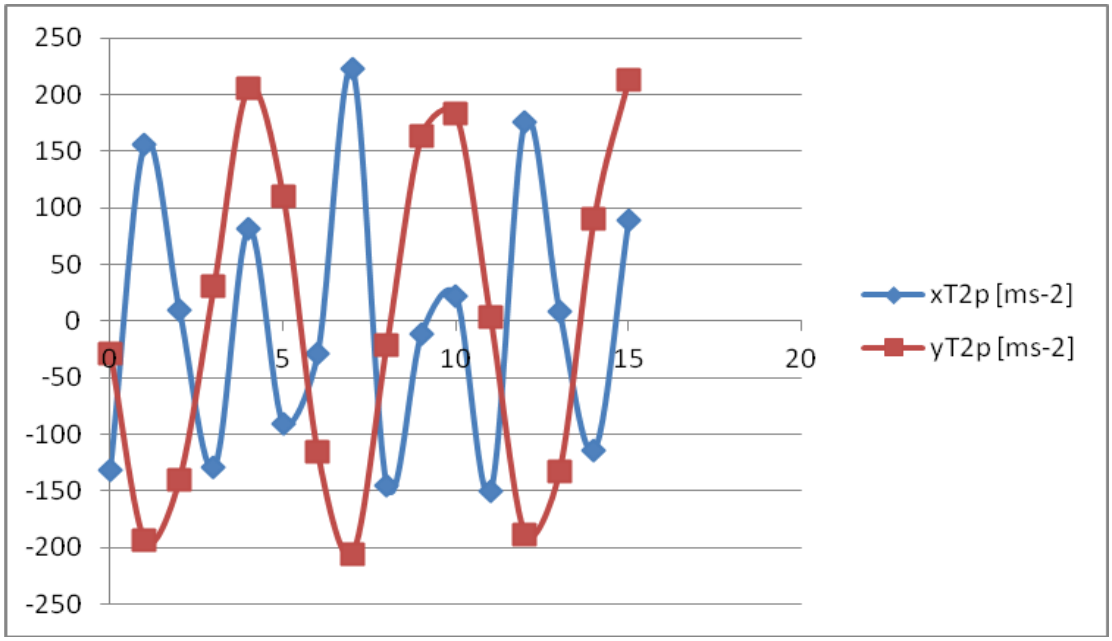


**Figure 21.** The accelerations of the coordinates of the point T end effector

It should be noted that in the calculations and in the presented diagrams, the final effector point was considered in the opposite part to the one in figure 1, according to its position indicated in figure 22.

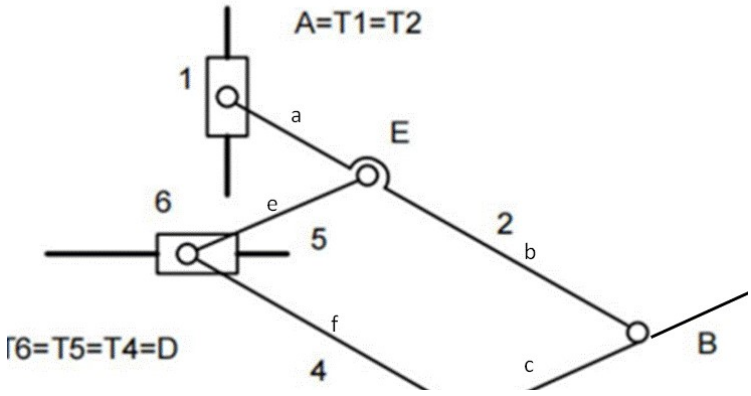


**Figure 22.** The kinematic scheme of the 2T6R plan robot presented with two cylindrical drive motors (the second variant, when the robot has the working arm oriented upwards)

## 4. Conclusions

The paper presented an original robot, 2T6R, with its structure, geometry, and direct kinematics, which generates the robot's trajectories and workspace, but also contributes directly to the complete dynamic calculations, including the forces acting on the robot's mechanism.

A robotic mobile mechanical system of this type has the advantage of simplicity in design, construction, and use, it can be used in various work environments, including industrial, with a generous workspace, simple and good dynamics, being easy to install, implemented, and maintained, very reliable, but very robust and well balanced for a serial mobile mechanical system.

This type of robot can be designed and built-in in various industrial sizes, it can work as a mini robot, as an average robot, but also as a heavyweight and oversized robot. Being very fast and dynamic (well balanced), it can be easily implemented.

The greatest difficulty in any type of industrial robot is represented by the actuators, which most often can produce blockages in operation, interruptions, deviations from the desired trajectory even in the conditions of a rigorously controlled command, variations, and dynamic vibrations, the reason for which the structure simple one presented has various advantages, the actuators for the proposed robot being from the three basic ones, a rotation of the main column as for any serial robot, and for the planar mechanism instead of two other rotations, as usual, it has two translation moves, two type actuators cylinder-piston, which at high loads will be mandatory two hydraulic cylinders, and at lower loads could be linear actuators (linear electric motors).

**Funding:**

a) 1-Research contract: 1-Research contract: Contract number 36-5-4D/1986 from 24IV1985, beneficiary CNST RO (Romanian National Center for Science and Technology) Improving dynamic mechanisms.

b) 2-Contract research integration. 19-91-3 from 29.03.1991; Beneficiary: MIS; TOPIC: Research on designing mechanisms with bars, cams, and gears, with application in industrial robots.

c) 3-Contract research. GR 69/10.05.2007: NURC in 2762; theme 8: Dynamic analysis of mechanisms and manipulators with bars and gears.

d) 4-Labor contract, no. 35/22.01.2013, the UPB, "Stand for reading performance parameters of kinematics and dynamic mechanisms, using inductive and incremental encoders, to a Mitsubishi Mechatronic System" "PN-II-IN-CI-2012-1-0389".

**Author Contributions:** Both authors have contributed equally to carry out this paper.

**Acknowledgments:** This text was acknowledged and appreciated by Dr. Veturia CHIROIU Honorific member of Technical Sciences Academy of Romania (ASTR) PhD supervisor in Mechanical Engineering.

**Conflicts of Interest:** "The authors declare no conflict of interest."

## References

1. FIT., Petrescu, 2008. "Theoretical and Applied Contributions About the Dynamic of Planar Mechanisms with Superior Joints", Doctoral Thesis.
2. K.Hain, Optimization of a cam mechanism to give good transmissibility maximal output angle of swing and minimal acceleration. J. Mechanisms 6(4) (1971) 419-434. doi:10.1016/0022-2569(71)90044-9
3. F. Giordana, V. Rognoni, G. Ruggieri, On the influence of measurement errors in the Kinematic analysis of cam. Mechanism Mach. Theory 14(5) (1979) 327-340. doi:10.1016/0094-114X(79)90019-3
4. P. Antonescu, F.I.T. Petrescu, Analytical method of synthesis of cam mechanism and flat stick. In: Proceedings of the Fourth International Symposium on Theory and Practice of Mechanisms, Vol. III-1, Bucharest, 1985.
5. P. Antonescu, F.I.T. Petrescu, D. Antonescu, Sinteza geometrică a mecanismului rotativ de camă și balansier. SYROM'97, București, 1997.
6. J. Angeles, C. Lopez-Cajun, Optimal synthesis of cam mechanisms with oscillating flat-face followers. Mechanism Mach. Theory 23(1) (1988) 1-6. doi:10.1016/0094-114X(88)90002-X
7. D. Taraza, N.A. Henein, W. Bryzik, The Frequency Analysis of the Crankshaft's Speed Variation: A Reliable Tool for Diesel Engine Diagnosis. J. Eng. Gas Turbines Power 123(2) (2001) 428-432. doi:10.1115/1.1359479
8. J.L. Wiederrich, B. Roth, Design of low vibration cam profiles. In: Cams and Cam Mechanisms. Ed. J. Rees Jones, MEP, London and Birmingham, Alabama, 1974.
9. G.F. Fawcett, J.N. Fawcett, Comparison of polydyne and non polydyne cams. In: Cams and cam mechanisms. Ed. J. Rees Jones, MEP, London and Birmingham, Alabama, 1974.
10. J.R. Jones, J.E. Reeve, Dynamic response of cam curves based on sinusoidal segments. In: Cams and cam mechanisms. Ed. J. Rees Jones, MEP, London and Birmingham, Alabama. 1974
11. D. Tesar, G.K. Matthew, The design of modeled cam systems. In: Cams and cam mechanisms, Ed. J. Rees Jones, MEP, London and Birmingham, Alabama, 1974
12. I. Sava, Contributions to Dynamics and Optimization of Income Mechanism Synthesis. Ph.D. Thesis, I.P.B., 1970

13. M.P. Koster, The effects of backlash and shaft flexibility on the dynamic behavior of a cam mechanism. In: Cams and cam mechanisms, Ed. J. Rees Jones, MEP, London and Birmingham, Alabama, 1974.
14. P. Antonescu, F.I.T. Petrescu, Contributions to kineto elastodynamic analysis of distribution mechanisms. SYROM 89, Bucharest, 1989
15. F.I.T. Petrescu, R.V. Petrescu, Cam Gears Dynamics in the Classic Distribution. Ind. J. Manag.Prod. 5(1) (2014) 166-185. doi:10.14807/ijmp.v5i1.133
16. F.I.T. Petrescu, R.V. Petrescu, An Algorithm for Setting the Dynamic Parameters of the Classic Distribution Mechanism. Int. Rev. Model. Simul. 6(5) (2013) 1637-1641.
17. F.I.T. Petrescu, R.V. Petrescu, Dynamic Synthesis of the Rotary Cam and Translated Tappet with Roll. Int. Rev. Model. Simul. 6(2) (2013) 600-607.
18. F.I.T. Petrescu, R.V. Petrescu, Cams with High Efficiency. Int. Rev. Mech. Eng. 7(4) (2013) 599-606.
19. F.I.T. Petrescu, R.V. Petrescu, Forces, and Efficiency of Cams. Int. Rev. Mech. Eng. 7(3) (2013) 507-511.
20. F.I.T. Petrescu, Geometric synthesis of distribution mechanisms. I have. J. Eng. Applic. Science. 8 (1) (2015) 63-81. DOI: 10.3844 / ajeassp.2015.63.81
21. F.I.T. Petrescu, equations of motion of machines for internal combustion heat engines. I have. J. Eng. Applic. Science. 8 (1) (2015) 127-137. DOI: 10.3844 / ajeassp.2015.127.137
22. F.I.T. Petrescu, Basics of analysis and optimization of rigid memory systems - course and applications. Create Space Publishing House, USA, (Romanian edition), 2012. ISBN 978-1-4700-2436-9
23. M.M. Mirsayar, V.A. Joneidi, R.V. Petrescu, F.I.T. Petrescu, F. Berto, 2017. Extended MTSN criterion for fracture analysis of soda-lime glass, Engineering Fracture Mechanics 178:50–59, http://doi.org/10.1016/j.engfracmech.2017.04.018
24. S. Wen, J. Zhu, X. Li, A. Rad, and X. Chen, 2012. End-point contact force control with quantitative feedback theory for mobile robots. IJARS, DOI: 10.5772/53742
25. F.I.T. Petrescu, R.V. Petrescu, 2016. Dynamic cinematic to a structure 2R. Revista Geintec-Gestao Inovacao E Tecnologias, 6(2):3143-3154. DOI: 10.7198/S2237-072220160002012
26. R.V. Petrescu, R. Aversa, A. Apicella, F.I.T. Petrescu, 2016. Future medicine services robotics. Am. J. Eng. Applied Sci., 9(4):1062-1087. DOI: 10.3844/ajeassp.2016.1062.1087
27. S. Tabaković, M. Zeljković, R. Gatalo, and A. Zivković, 2013. Program suite for conceptual designing of parallel mechanism-based robots and machine tools. Int. J. Advanced Robotic Sys., DOI: 10.5772/56633
28. K. Wang, M. Luo, T. Mei, J. Zhao, and Y. Cao, 2013. Dynamics analysis of a three-DOF planar serial-parallel mechanism for active dynamic balancing with respect to a given trajectory. Int. J. Advanced Robotic Sys., DOI: 10.5772/54201
29. M. Garcia-Murillo, J. Gallardo-Alvarado, and E. Castillo-Castaneda, 2013. Finding the generalized forces of a series-parallel manipulator. IJARS, DOI: 10.5772/53824
30. W. Lin, B. Li, X. Yang, and D. Zhang, 2013. Modelling and control of inverse dynamics for a 5-DOF parallel kinematic polishing machine. Int. J. Advanced Robotic Sys., DOI: 10.5772/54966
31. B. He, Z. Wang, Q. Li, H. Xie, and R. Shen, 2013. An analytic method for the kinematics and dynamics of a multiple-backbone continuum robot. IJARS, DOI: 10.5772/54051
32. H. Liu, W. Zhou, X. Lai, and S. Zhu, 2013. An efficient inverse kinematic algorithm for a PUMA560-structured robot manipulator. IJARS, DOI: 10.5772/56403
33. W. Cao, H. Ding, Z. Bin, and C. Ziming, 2013. New structural representation and digital-analysis platform for symmetrical parallel mechanisms. Int. J. Advanced Robotic Sys., DOI: 10.5772/56380
34. X. Tang, D. Sun and Z. Shao, 2013. The structure and dimensional design of a reconfigurable PKM. IJARS, DOI: 10.5772/54696
35. G. Tong, J. Gu, and W. Xie, 2013. Virtual entity-based rapid prototype for design and simulation of humanoid robots. Int. J. Advanced Robotic Sys., DOI: 10.5772/55936
36. BJ. Lee, 2013. Geometrical derivation of differential kinematics to calibrate model parameters of flexible manipulator. Int. J. Advanced Robotic Sys., DOI: 10.5772/55592
37. F. Padula, and V. Perdereau, 2013. An on-line path planner for industrial manipulators. Int. J. Advanced Robotic Sys., DOI: 10.5772/55063
38. S. Perumaal, and N. Jawahar, 2013. Automated trajectory planner of industrial robot for pick-and-place task. IJARS, DOI: 10.5772/53940
39. H. Dong, N. Giakoumidis, N. Figueroa, and N. Mavridis, 2013.
40. R. Aversa, F. Tamburrino, R.V. Petrescu, F.I.T. Petrescu, M. Artur, G. Chen, A. Apicella, 2016. Biomechanically Inspired Shape Memory Effect Machines Driven by Muscle like Acting NiTi Alloys, Am. J. Applied Sci. 13(11):1264-1271. DOI: 10.3844/ajassp.2016.1264.1271
41. Approaching behaviour monitor and vibration indication in developing a General Moving Object Alarm System (GMOAS). Int. J. Advanced Robotic Sys., DOI: 10.5772/56586